Nudging axially compressed cylindrical panels towards imperfection insensitivity

B. S. Cox*
Materials and Structures Research Centre,
Department of Mechanical Engineering,
University of Bath,
Bath, BA2 7AY, UK
Email: B.S.Cox@bath.ac.uk

R. M. J. Groh
Bristol Composites Institute (ACCIS),
University of Bristol,
Bristol, BS8 1TR, UK
Email: Rainer.Groh@bristol.ac.uk

A. Pirrera
Bristol Composites Institute (ACCIS),
University of Bristol,
Bristol, BS8 1TR, UK
Email: Alberto.Pirrera@bristol.ac.uk

ABSTRACT

Curved shell structures are known for their excellent load-carrying capability and are commonly used in thin-walled constructions. Although theoretically able to withstand greater buckling loads than flat structures, shell structures are notoriously sensitive to imperfections owing to their post-buckling behaviour often being governed by subcritical bifurcations. Thus, shell structures often buckle at significantly lower loads than those predicted numerically and the ensuing dynamic snap to another equilibrium can lead to permanent damage. Furthermore, the strong sensitivity to initial imperfections, as well as their stochastic nature, limits the predictive capability of current stability analyses. Our objective here is to convert the subcritical nature of the buckling event to a super-critical one, thereby improving the reliability of numerical predictions and mitigating the possibility of catastrophic failure. We explore the elastically nonlinear post-buckling response of axially compressed cylindrical panels using numerical continuation techniques. These analyses show that axially compressed panels exhibit a highly nonlinear and complex post-buckling behaviour with many entangled post-buckled equilibrium curves. We unveil isolated regions of stable equilibria in otherwise unstable post-buckled regimes, which often possess greater load-carrying capacity. By modifying the initial geometry of the panel in a targeted—rather than stochastic—and imperceptible manner, the post-buckling behaviour of these shells can be tailored without a significant increase in mass. These findings provide new insight into the buckling and post-buckling behaviour of shell structures, and opportunities for modifying and controlling their post-buckling response for enhanced efficiency and functionality.

1 Introduction

In many engineering disciplines the onset of geometric nonlinearity is considered a form of structural failure. However, over the last decade an alternative perspective has emerged that recognises the positive effects of embracing structural nonlinearities, particularly elastic instabilities [See the following review papers: 1, 2]. This alternative vision aims to expand the structural design space by taking advantage of instabilities purposely tailored to be controlled and predictable. In this manner, embracing nonlinearities facilitates a new class of *well-behaved* nonlinear structures with improved functionality [3]. From macro-scale morphing structures [4, 5], to meso-scale energy harvesting [6, 7], and micro-scale microelectromechanical systems [8], structural nonlinearities are increasingly being sought as positive features.

Owing to their structural efficiency, shell structures, are of core and central interests to this emerging design paradigm, across a range of disciplines. However, in order for shell structures to be considered *well-behaved*, their buckling and post-buckling behaviour needs to be fully understood and controlled.

*Corresponding author.

The buckling and post-buckling of shell structures has a been of interest for a long time. So much so that the topic is inextricably linked to many of the great structural mechanicians of the 20th century (Timoshenko, von Kármán, Koiter, Budiansky, *etc*.). In particular, the susceptibility of shell structures to sudden buckling failure, well below the theoretically predicted linear buckling load, has been debated for many decades [9]. Although a number of factors, such as boundary conditions, loading imperfections and material variations account for some of the discrepancies, the work of Koiter [10], and Arbocz and Babcock [11] showed that geometric imperfections are the main culprit. Furthermore, the effect of imperfections on load buckling resistance was shown to be relevant to general thin-walled structures [12]. To this day, for the lack of better alternatives, engineers rely on empirically-derived and often conservative knock-down factors [13].

Another approach to mitigate premature buckling failure in shell structures is to overcome the source of the underlying imperfection sensitivity: subcritical bifurcations. By modifying certain geometrical or material features, the post-buckling response can be changed from subcritical to supercritical, and in theory mitigate the effects of imperfection sensitivity. Several recent studies have illustrated the benefits of an applied geometric change to the baseline structure. Mang et al. [14] and Schranz et al. [15] successfully realised a conversion from imperfection-sensitivity to imperfection-*in*sensitivity by: (i) altering the thickness of certain structural components; (ii) attaching auxiliary members to the structure, such as springs; (iii) and by altering key geometric dimensions, *e.g.* the rise of an arch. Although successful in mitigating imperfection sensitivity, these approaches often render the altered structure less useful in operation. Limitations include: geometrical space constraints that may prevent the use of auxiliary components; the constraint that certain structures do not lend themselves to the attachment of other components; or the fact that key dimensions are typically fixed *a priori*. In a similar vein, Ning and Pellegrino [16, 17] designed a cylindrical shell with a wavy cross-section to ensure the structure is less sensitive to imperfections. However, since the shape of shell structures is often defined by operational specifications, a wavy cylinder may no longer be useful for its intended use, *e.g.* as a cylindrical rocket structure. Most promisingly, a research group at Michigan State University have shown that the elastic post-buckling response of cylinders can be modified by providing large and strategically designed imperfections [18, 19, 2, 20, 21, 22] in the form of seeded geometric alterations.

Simultaneously, the increasing adoption of composite materials has improved the ability to control the buckling and post-buckling behaviour of shell structures by means of material tailoring. For example, White and Weaver [23] provide an interesting approach based on steering the fibre reinforcement along curvilinear paths over a cylindrical shell surface. In this manner, curved shell structures with stable, plate-like post-buckling behaviour were designed.

Although, cylindrical shells are common in many civil and aerospace applications, research interest also extends to toroidal, torispherical and domed structures. Bielski [24] analysed toroidal shell structures and concluded that it is possible to maintain a stable post-buckled response with an ovalisation of the meridional section. Lu et al. [25] analysed the effects of increasing the magnitude of applied imperfections on torispherical pressure vessels. They concluded that beyond a specific particular imperfection-magnitude, the structural response increases in compliance but converges to the same equilibrium response irrespective of additional increases in imperfection magnitude. More recently, Lee et al. [26] evaluated the critical response of spherical elastic shells under pressure loading with an emphasis on how knockdown factors are affected by an engineered dimple-like imperfection. Their work draws attention to the fact that there exists a direct relationship between the critical buckling load and the geometry of the applied imperfection (amplitude, angular width, *etc.*). Both Finite Element (FE) simulations and a semi-analytical model were able to accurately predict the knockdown factors of these imperfect spherical shells, illustrating that their behaviour can be described with certainty once the initial geometry, including dominant imperfections, is defined precisely.

1.1 Aims and objectives

The aim of this manuscript is twofold. First, we elucidate the complex response of shell structures and illustrate that there exist a plethora of secondary critical points and entangled equilibrium paths in close proximity to the first critical buckling point. Second, we show that undertaking a full exploration of the structural response deep into the post-buckled regime—far beyond what is conventionally conducted—can reveal potentially useful stable equilibria that possess greater load-carrying capacity and compliance than the natural bifurcation behaviour of the structure would otherwise permit. These attractive stable states are normally inaccessible as they are separated from the natural response of the structure by unstable equilibrium paths. Here, to connect and exploit these paths we apply a previously introduced design framework known as *modal nudging* [27]. Modal nudging uses the deformation modes associated to these stable post-buckled equilibria to alter the undeformed baseline geometry of the structure imperceptibly, thereby favouring the seeded post-buckling response over potential alternatives. Modal nudging has never been applied to shell-like structures before, and by applying modal nudging it is possible to alter the response of curved panels from the baseline subcritical response, often associated with imperfection-sensitivity, to a well-behaved, imperfection-insensitive supercritical response (as illustrated in Figure 1).

The remainder of this paper is structured as follows. Section 2 introduces the problem, *i.e.* two identical cylindrical panels subjected to an axial compressive load, each with different boundary conditions: (i) pinned; (ii) and clamped-pinned. A validation of preliminary results, which is undertaken using the commercial finite element analysis software ABAQUS, is also included. Section 3 provides a comprehensive discussion of the baseline response of both shell models and includes

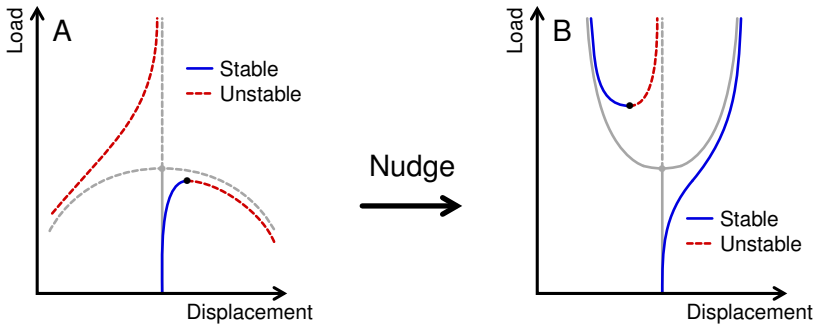

Fig. 1: Perfect and imperfect bifurcation branching responses: (A) Subcritical; (B) Supercritical. [27]

a number of figures illustrating the complexity manifest in the full spectrum of equilibrium paths. In section 4, the modal nudging technique is employed to favourably alter the response of the cylindrical panels. This is followed in section 5 by a brief discussion of the significance of the results with regards to the static-dynamic analogy of "chaotic" solutions in boundary value problems and initial value problems. We close with section 6 in which conclusions are drawn.

2 Model definition

The structural response of two axially-compressed cylindrical panels, of identical geometry and previously studied by Jun and Hong [28, case $L/R = 1$, $d/L = 1.047$], is evaluated herein (see Figure 2). For the first model (Figure 2A), all four edges are pinned and this load case is henceforth referred to as "PPPP" (Pinned-Pinned-Pinned-Pinned). The second model has its curved edges clamped (Figure 2B) and is thus given the designation "CCPP" (Clamped-Clamped-Pinned-Pinned). To mimic typical experimental loading, an in-plane edge load on one of the curved sides is introduced via displacement control (rigid loading).

The material and geometric properties for both cylindrical panels are summarised in Table 1, where E is the isotropic Young's modulus of elasticity, ν is the Poisson's ratio, t the shell thickness, r the radius of curvature, L the longitudinal length, and s the total arc-length. The panels are analysed using an in-house MATLAB-based finite element code [3], which makes use of nonlinear degenerated shell elements based on the complete Green-Lagrange strain tensor and formulated in a total Lagrangian framework. The finite element models are constructed with 43×43 16-node elements with shell director parametrisation as introduced by Ramm [29]. Thus, the shell elements are geometrically nonlinear and can model deformations with small strains but large rotations of the shell normals (large curvatures as long as elastic limit is not exceeded).

A model validation of the pre-buckling and initial post-buckling response of both panels was conducted using ABAQUS with a mesh of 100×100 S8R elements (201×201 nodes) employing the in-built Riks [30] arc-length solver. The model consists of imposing an initial imperceptible imperfection in the form of the first buckling eigenmode in order to follow the corresponding branching path. The validation results, in terms of normalised edge reaction load $\bar{R} = R/\lambda_{\text{crit}}$ *vs* normalised end-shortening $\bar{w} = w/t$, are presented in Figure 3, where R is the total edge reaction load, w is the applied uniform displacement along one edge, and λ_{crit} is the first buckling load (3.973×10^4 N and 4.280×10^4 N for PPPP and CCPP, respectively). The broken black lines correspond to ABAQUS results. Values from the in-house MATLAB code are colour-coded with blue representing stable equilibria, red unstable equilibria, and black dots denoting critical points (limit or branching points). The pre-buckling, buckling and initial post-buckling response have therefore been successfully validated. Mesh convergence studies were conducted in order to ensure no divergence occurs for the deep post-buckled paths, but it is not possible to validate these deeper post-buckled paths using a commercial FE package, as, to the authors knowledge, no commercial FE package offers the required capabilities. For instance, the analyst has very limited control over the equilibrium path that is being traced, such that unwanted path-jumping typically occurs. As a viable alternative, the in-house MATLAB-based FE code [3] has been employed as it has been validated on various occasions against commercial FE packages (as much as these allow given the lack of comparable capabilities), other results in literature, and also experimental results—the interested reader is encouraged to study these selected examples [31, 32, 33].

3 Baseline structural response of cylindrical panels

The baseline normalised load-displacement response for panel PPPP is presented in Figure 4, where the stability of each equilibrium path is highlighted (red for unstable equilibria and blue for stable equilibria). The solution depicted in Figure 4A is the complete solution of the fundamental path and is therefore a single equilibrium curve with no additional branching

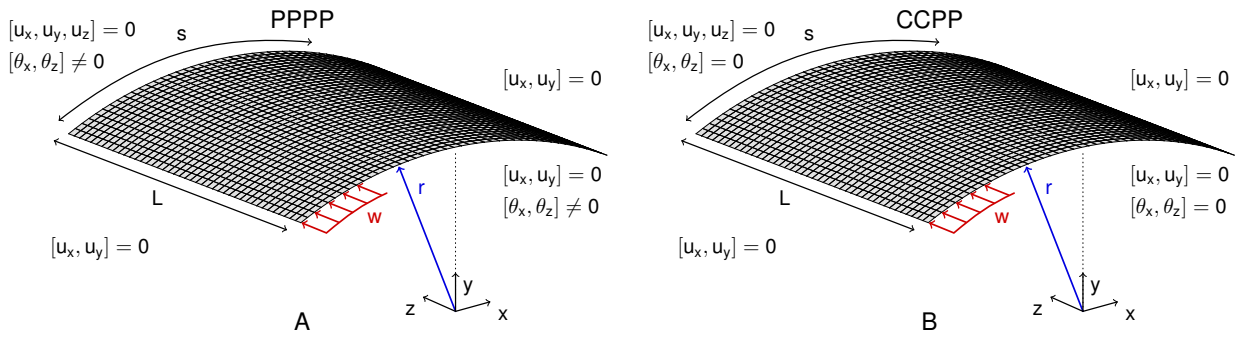

Fig. 2: Axially compressed cylindrical panel with geometric dimensions and imposed boundary conditions: (A) Pinned-Pinned-Pinned-Pinned (PPPP) edges, where rotations are free at each edge; (B) Clamped-Clamped-Pinned-Pinned (CCPP) edges, where rotations are constrained on the curved sides.

Table 1: Cylindrical panel geometric dimensions and material properties for both PPPP and CCPP load cases.

E (Nmm^{-2})	ν (-)	t (mm)	r/t	L/r	s/L
7×10^4	0.25	1	150	1	1.047

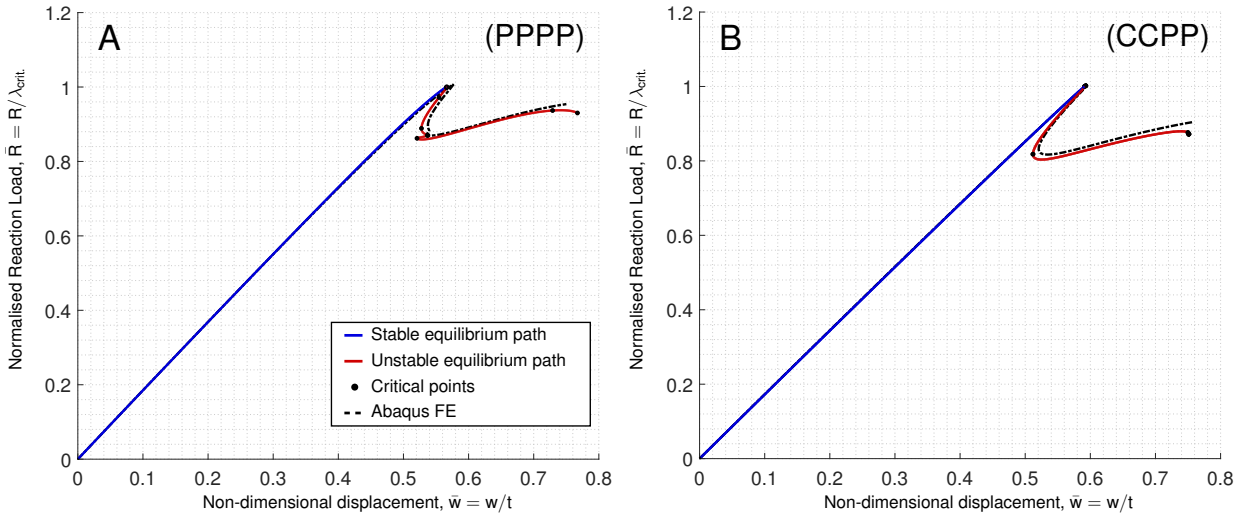

Fig. 3: Initial load-displacement response of (A) PPPP; and (B) CCPP panels solved using an in-house MATLAB-based nonlinear finite element analysis. Validation is provided with equivalent ABAQUS models (dashed black lines).

paths traced. Figure 4B is an identical plot to Figure 4A, however in this instance the stable (blue) regions are further emphasised for clarity. It is evident that an additional five stable regions exist deep in the post-buckling regime beyond the initial linear pre-buckling response. Physically, each of these stable equilibrium paths represent a physical deformation shape, but since they are isolated from the pre-buckling path by unstable branch segments, they are unattainable in practice. In order to observe these additional stable states physically, one could load the panel until the first critical buckling point is reached and expect the shell to then snap on to one of these stable regions. However, it is not obvious which of the stable regions is the preferential attractor, if any in a dynamic scenario. Additionally, the shell may deform plastically or break upon dynamic snap.

Figure 4A shows that the post-buckling behaviour is split into two clusters of entangled equilibrium paths. These two clusters, one close to the first instability on the pre-buckling path and the other deep in the post-buckling region, are shown in Figures 4C–D and Figures 4E–F, respectively. These responses are practical examples of the complex shell-like behaviour described by, for instance, Thompson [34]. Figure 4C and Figure 4E illustrate the large number of critical points, highlighted by the black dots. In this particular model, 243 branching points and 65 limit points exist. Limit points are

minima and maxima of the equilibrium paths where a stabilising or destabilising mode is introduced in the deformation field. Branching points denote locations where two or more equilibrium paths intersect at the same total potential energy.

The stable (blue) regions highlighted in the deep post-buckling region of Figure 4B and Figure 4F are interesting as they suggest that the structure is capable of carrying a greater load deep into the post-buckled regime. As mentioned in Section 2, these stable states cannot be obtained simply by compressing the shell from the unloaded state, as they are separated from the pre-buckling response by unstable equilibria. In section 4 we show that with modal nudging it is possible to take advantage of this latent load-carrying capacity. In this way, analyses that uncover the deep post-buckling response of structures—typically considered a computationally expensive analysis of little value—obtain a new impetus as they can reveal residual load-carrying capacity.

Similarly, the baseline response for model CCPP is presented in Figure 5, where Figure 5A is the complete fundamental path with no additional branching paths traced. Figure 5B provides a clearer depiction of the stable solutions deep into the post-buckled response. These results once again illustrate the complexity of the possible post-buckling behaviour with a large number of critical points. In this particular model, 407 branching points and 73 limit points exist. For the PPPP load case (Figure 4D,F), the stable segments are relatively extended, whereas, for the CCPP load case (Figure 5D,F), two larger stable regions exist with the remaining stable equilibria being small and clustered (See Figure 5F).

To further emphasise this complex behaviour, consider the branching paths presented in Figures 6 and Figures 7. These equilibrium curves extend the baseline response depicted in Figures 4 and 5, respectively, to include symmetry-breaking equilibria. Note that although there exist hundreds of branching points and intersection branching paths along each of the two fundamental paths (PPPP and CCPP), only those exhibiting stable equilibria are presented in Figures 6 and 7. Of the branching paths that are not shown in Figures 6 and Figures 7, the vast majority contain additional critical points, most of which present additional branching points, leading to further paths still. To explore the entire domain therefore becomes an unassailable task. According to the definition of Kocsis and Károlyi [35] this exponential increase in equilibrium paths (stable or unstable) as a result of continuous branching, is an example of "spatial" chaos.

It is evident by comparison of the results for the PPPP panel in Figure 6 to those for the CCPP panel in Figure 7 that, for the latter, there are significantly fewer stable regions in the post-buckled regime. Crucially for the perspective of modal nudging, there exists no stable region in the CCPP response along branched paths with increased load-carrying capacity beyond that of the pre-buckling solution. Figure 6 presents a total of eighteen unique branching paths that have signs of stability, whereas, for the CCPP panel in Figure 7, there are only four unique branching paths that present signs of stability, and all of these have significantly less loading capacity, albeit with an increased compliance.

4 Modal nudging of the baseline structural response

Initial geometric imperfections are often imposed in structural instability analyses to determine reduced buckling loads that are closer to the real-world response. For supercritical bifurcations with an initially stable post-buckling response, the effects of initial imperfections are relatively benign as they round-off the branching point (see Figure 1B) and do not lead to a large knock-down effect. For subcritical bifurcations, as observed in many shell structures, imperfections lead to a large knock-down effect and a dynamic transition to alternative equilibria. Generally speaking, any stochastic imperfection reduces the capacity of imperfection-sensitive structures, although specific imperfection shapes, such as imperfections based on linear combinations of the first few critical eigenvectors, can also lead to a pronounced knock-down on load-carrying capacity. The perturbations applied in modal nudging [27] differ in that the small geometric changes are (i) deterministically imposed; and (ii) do not lead to reduced structural capacity, but to an entirely new structural response. In many cases, this new "nudged" structural response improves the load-carrying capacity, compliance, stability and efficiency of the structure. Therefore this geometry changes (the nudges) cannot be viewed as unwanted geometric imperfections but rather as positive additions to the design of a structure.

To embrace the post-buckling response of shell structures fully, and to improve structural performance in the process, we will hence adopt the previously introduced technique of modal nudging. Of the many different stable states deep within the post-buckled regime, both from the fundamental path and from the branched paths, any could be chosen for nudging. However, only eight stable states are chosen here. The PPPP (Figure 4 and Figure 6) panel presents a greater opportunity for nudging than the CCPP panel (Figure 5 and Figure 7). Therefore six states are selected from the PPPP response and two more from the CCPP response. The location of the selected states on the equilibrium curves is illustrated in Figure 8. The corresponding mode shapes are presented in Figure 9. The modes are selected as they all possess a response capable of carrying greater load than the original linear pre-buckling response. This is further highlighted in Table 2, where the "start point" is considered to be the end of the stable region nearest to the reference state (zero load and zero displacement). In Table 2, it is evident that state-VI has the greatest potential capacity, for both total load and compliance, with a potential normalised load of $\bar{R} = 2.485$ and a compliance of $\bar{w} = 16.63$ (compared to the unnudged first buckling point at $\bar{R} = 1$ and $\bar{w} = 0.57$). However, it also potentially provides the greatest energy barrier as its "start point" is the furthest away from the reference state.

In a similar vein to Cox et al. [27], on discovering a potentially desirable equilibrium beyond the first instability point,

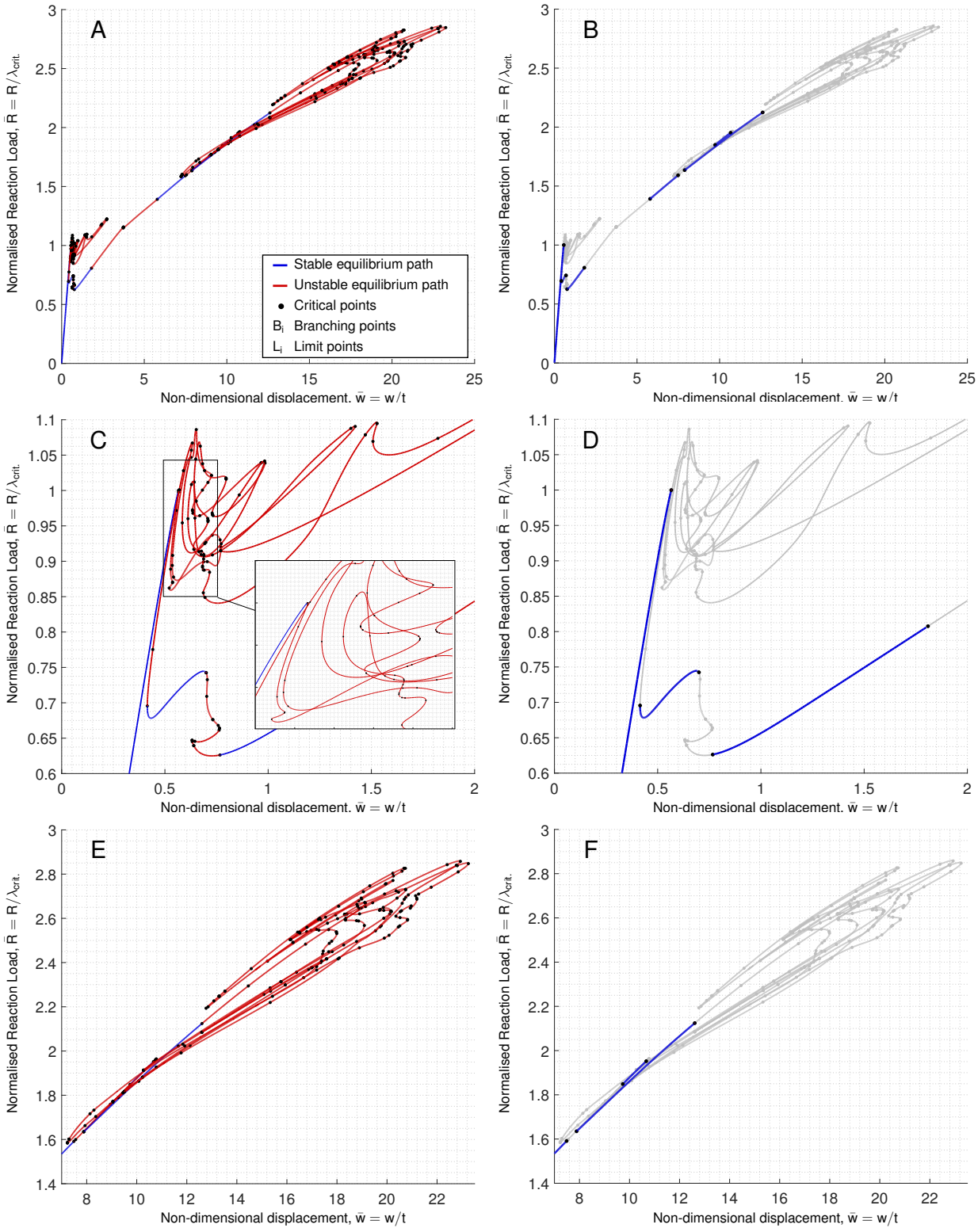

Fig. 4: The load-displacement response for the Pinned-Pinned-Pinned-Pinned (PPPP) model. (A) illustrates a single equilibrium path starting from the unloaded state, which exhibits multiple instabilities and entanglement. (B) is an identical plot to (A) with the stable solutions highlighted. (C) is a close-up view of the nonlinear response in the vicinity of the first critical point. (D) illustrates the stable solutions in the close-up view (C). (E) is a close-up view of the deep post-buckled region, and (F) illustrates the stable regions within this deep post-buckled region.

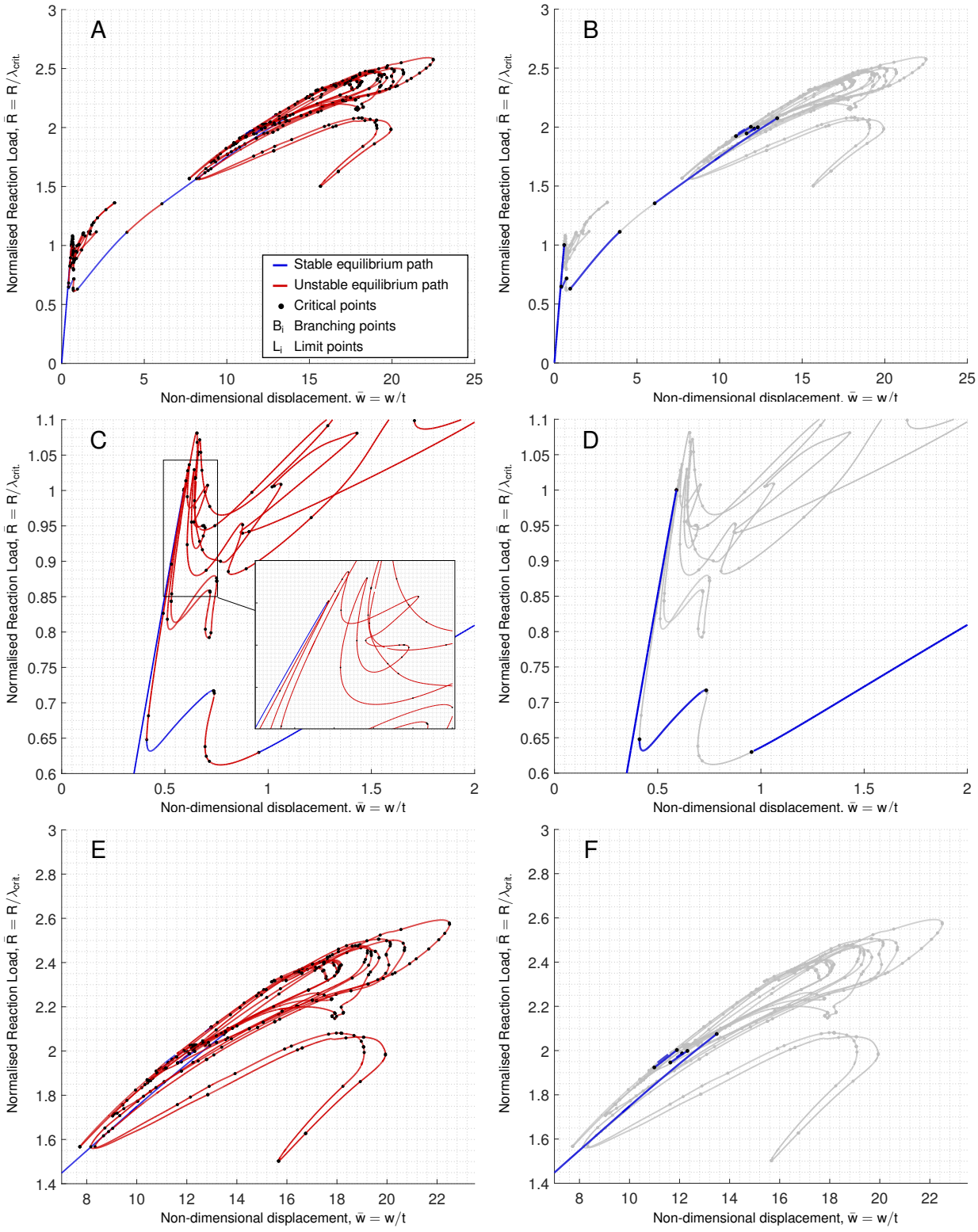

Fig. 5: The load-displacement response for the Clamped-Clamped-Pinned-Pinned (CCPP) model. (A) illustrates a single equilibrium path starting from the unloaded state, which exhibits multiple instabilities and entanglement. (B) is an identical plot to (A) with the stable solutions highlighted. (C) is a close-up view of the nonlinear response in the vicinity of the first critical point. (D) illustrates the stable solutions in the close-up view (C). (E) is a close-up view of the deep post-buckled region, and (F) illustrates the stable regions within this deep post-buckled region.

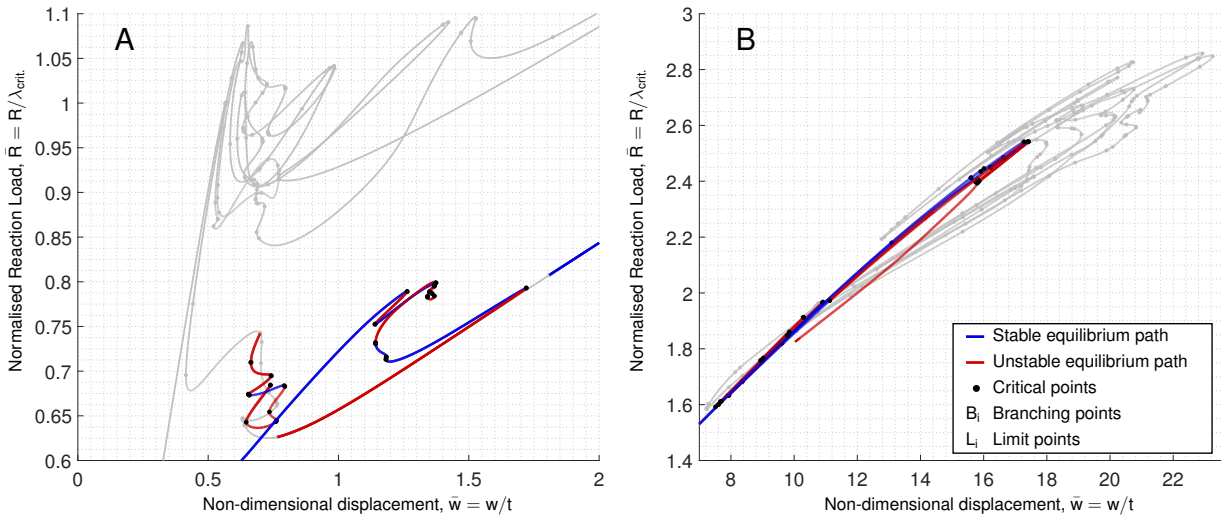

Fig. 6: Stable secondary paths for the PPPP load case, which branch from the fundamental path depicted previously in Figure 4. A total of eighteen branching paths are presented. There exist many other paths, but to the authors' knowledge, the paths shown are the only bifurcated paths that present stable solutions, and hence a potential opportunity for modal nudging. In (B) thirteen equilibrium paths are presented, the majority of which have similar responses. The grey curves correspond to the original baseline response of the PPPP panel previously shown in Figure 4.

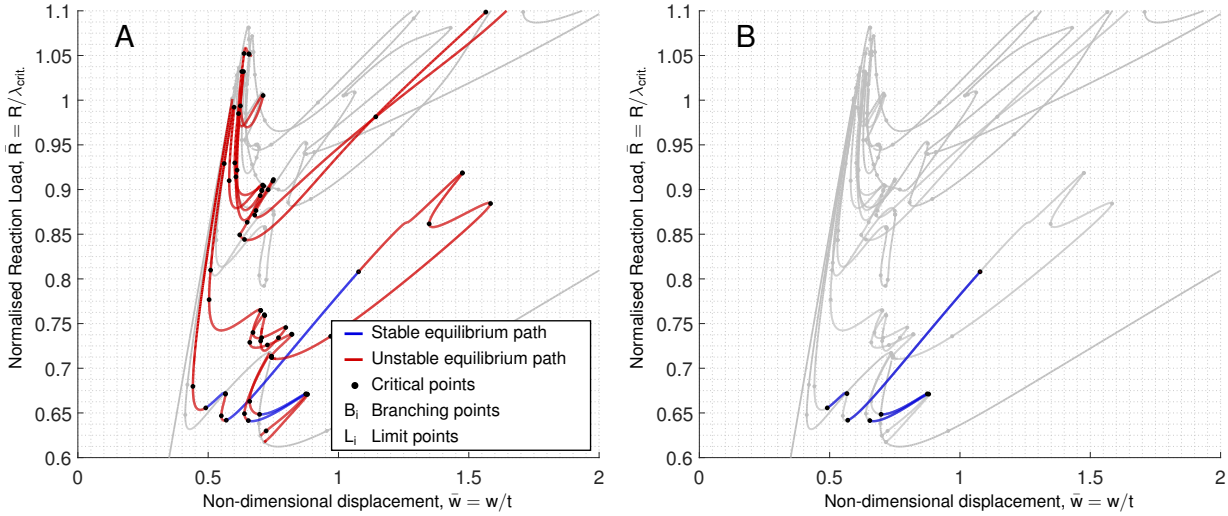

Fig. 7: Stable secondary paths for the CCPP load case, which branch from the fundamental path depicted previously in Figure 5 (A) Illustrates three bifurcation (branching) paths in with stable (blue) and unstable (red) regions highlighted; and (B) highlights these stable regions further. There exist many other paths, but to the authors' knowledge, the paths shown are the only bifurcated paths that present stable solutions, and hence a potential opportunity for modal nudging. The grey curves correspond to the original baseline response of the CCPP panel previously shown in Figure 5.

the deformation mode, $\mathbf{u}_{\text{state}}$, is extracted for any state along the desirable stable branch. This state is then used to alter the original, undeformed geometry, $\mathbf{x}_0$, of the structure. Hence,

$$\mathbf{x}_{\text{nudged}} = \mathbf{x}_0 + \eta \bar{\mathbf{u}}_{\text{state}}, \tag{1}$$

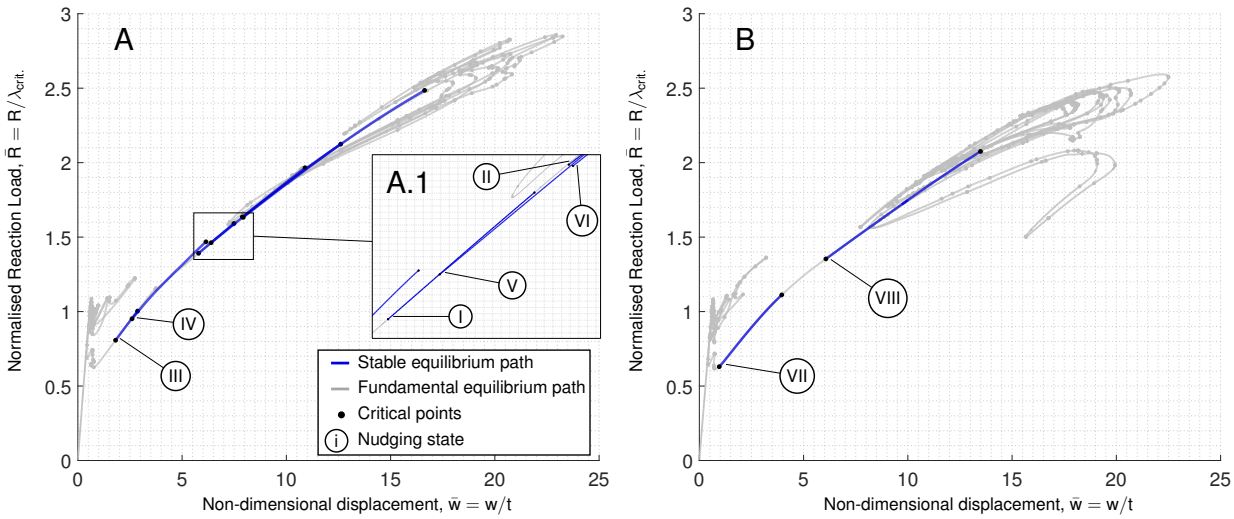

Fig. 8: Highlighted stable regions for nudge-state selection: (A) PPPP, states I–VI; (B) CCPP, states VII–VIII. States I, II, VII and VIII are stable regions on the fundamental paths, and states III-VI are stable regions on branching paths.

with

$$\bar{\mathbf{u}}_{\text{state}} = \frac{\mathbf{u}_{\text{state}}}{\|\mathbf{u}_{\text{state}}\|_2}, \tag{2}$$

and

$$\eta \|\bar{\mathbf{u}}_{\text{state}} \oslash \mathbf{x}_0\|_2 \ll 1, \tag{3}$$

where η is the non-dimensional nudging parameter, and $\oslash$ is the Hadamard division operator defined by $C_i = A_i/B_i$ with the subscript denoting the i^{th} component of the vector. The magnitude of the nudging parameter will vary from structure to structure and from mode shape to mode shape, but for all nudges in this manuscript Eq. (3) holds. For a structure where Eq. (3) is not valid, the corresponding geometrical change can no longer be classified as a nudge, but rather as generating an entirely new structure in its own right with its own unique structural response.

Figure 9 shows that all of the states chosen, correspond to nearly-identical mode shapes, albeit with minor variations. The large indentation at the centroid is the most significant feature, but equally are the four smaller indentations at each corner. Each of the eight nudges is applied to both PPPP and CCPP panels, the results of which are presented graphically in Figures 10A–H and Figures 11A–H, respectively.

4.1 Nudging a cylindrical panel: Pinned-Pinned (PPPP)

For the PPPP panel, on nudging to state-I, Figure 10A indicates that a compliant, controlled and stable response is possible. Provided that elasticity is maintained, this results in a structure whose load-carrying capacity ($\bar{R} = 2.056$) has increased to more than twice the unnudged response ($\bar{R} = 1$). This response is achieved with a nudging parameter value of $\eta = 13.5$, which equates to a maximum geometric alteration of $\bar{u}_\eta = 0.760$, where $\bar{u}_\eta = \max(\eta|\mathbf{u}_{\text{state}}|)/t$, *i.e.* a maximum geometric change of less than the shell thickness. This magnitude of the geometrical alteration of the nudge mode is observed at the centroid of the panel.

On nudging to state-II, as illustrated in Figure 10B, we recover an even greater load-carrying capacity ($\bar{R} = 2.135$) and compliance ($\bar{u} = 12.72$), which is achieved with a minor change in initial geometry ($\bar{u}_\eta = 0.844$). Nudging the response of panel PPPP to state-III results in an interesting response compared to all others nudges (See Figure 10C). In this case, two folds exist on the nudged equilibrium path, which hence features an unstable "snap-back" portion. This suggests that the shell is likely to undergo a small snap to the neighbouring stable path and continue to carry additional load. If this was to occur in practise, the loading capacity could increase to $\bar{R} = 1.880$ and $\bar{w} = 9.912$. Further validating this behaviour would require verification by means of a dynamic analysis.

Nudging to state-IV and state-V (see Figure 10D,E) also results in increased load-carrying capacities of $\bar{R} = 1.481$ and $\bar{R} = 2.092$, respectively, with complimentary increases in end-shortening compliance of $\bar{w} = 6.11$ and $\bar{w} = 12.07$. For the

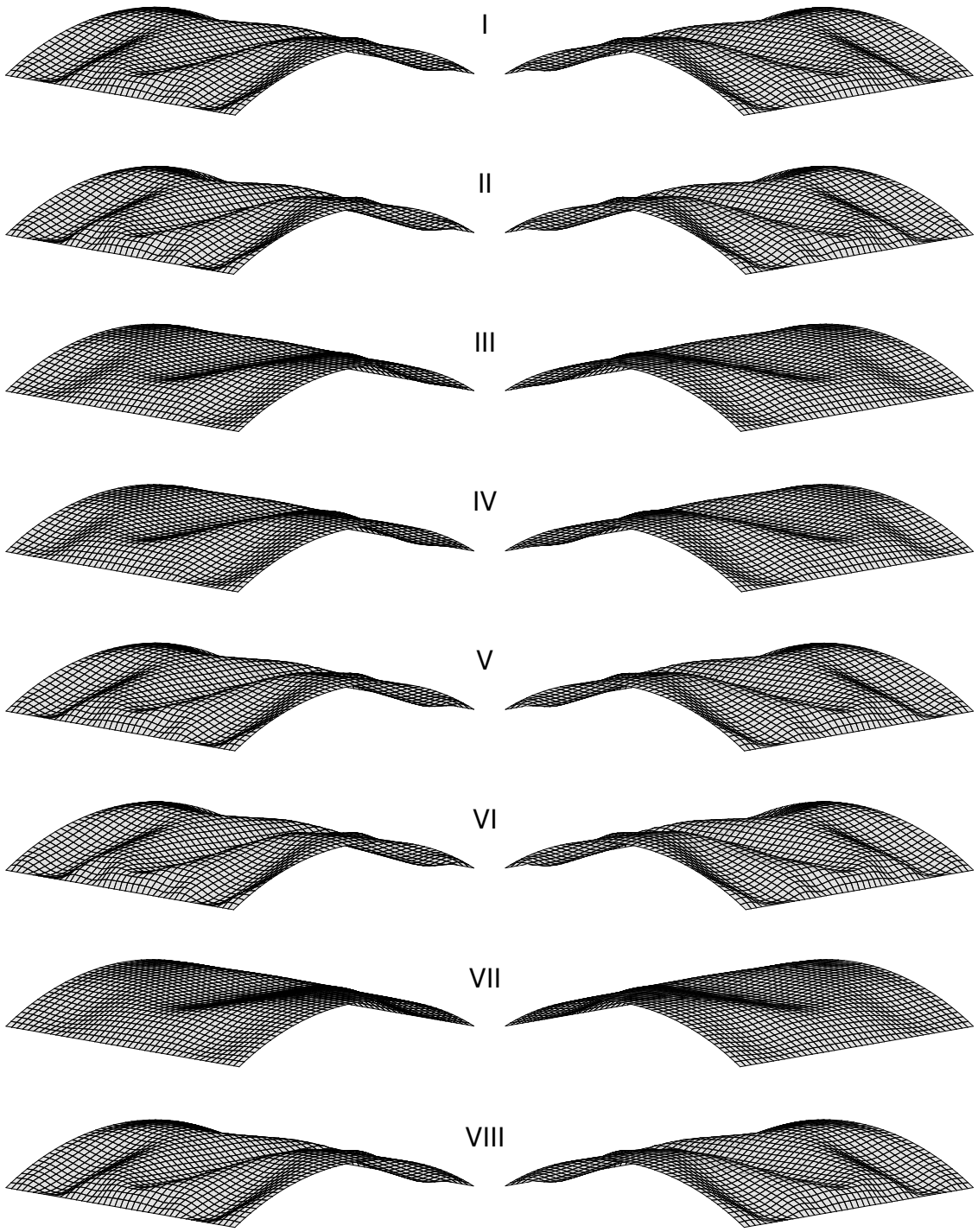

Fig. 9: Mode shapes used in nudging. Each figure represents the actual mode shape from the selected stable regions and therefore the absolute deformation before normalisation for the nudging procedure. States I–VI are each selected from the PPPP response and the final two states VII & VIII are selected from the CCPP response.

nudge to state-IV, this relates to a maximum geometric alteration of $\bar{u}_\eta = 0.735$, and for nudging to state-V, a maximum alteration of $\bar{u}_\eta = 0.738$.

The results also show that it is possible to nudge the PPPP panel using state-VI and state-VIII from the CCPP response. This is illustrated in Figure 10G and Figure 10H. Interestingly, the nudged responses do not correspond exactly to the "start point" and "end point" (see Table 2) of the original stable regions from the baseline response. The majority of the nudged

Table 2: Baseline response of the eight chosen nudge states, highlighting the start and end positions of each equilibrium path. Note that the "start" point corresponds to the end closest to the origin, and the "end point" corresponds to the end furthest from the origin. $\bar{R} = R/\lambda_{\text{crit}}$ is the normalised edge reaction load, and $\bar{w} = w/t$ is the normalised end-shortening.

	Start point		End point	
State	$\bar{R}$	$\bar{w}$	$\bar{R}$	$\bar{w}$
PPPP	0	0	1	0.57
CCPP	0	0	1	0.59
I	1.392	5.791	1.591	7.486
II	1.637	7.906	2.124	12.61
III	0.808	1.809	1.003	2.863
IV	0.951	2.599	1.468	6.145
V	1.462	6.389	1.966	10.90
VI	1.633	7.933	2.485	16.63
VII	0.630	0.955	1.112	3.954
VIII	1.354	6.069	2.075	13.48

responses shows a trend of increasing the load-carrying potential beyond the "end point" of these selected regions, and all are shown to exceed the initial buckling load of the baseline response.

Each plot in Figures 10A–H shows the deformation mode assumed by the shell in the corresponding analyses, with this shape observed at approximately $\bar{w} \approx 10.0$ where possible. For nudges to state-IV, state-VII, and state-VIII, the shapes correspond to $\bar{w} \approx 6.1$, 8.6, and 7.8, respectively, due to their lower compliance. On nudging to any path, the initial deformation of each panel is similar and transitions to the nudged mode shape only at the point of the visible kink in the response, which appears at $\bar{R} \approx 0.5$ for each nudge.

As shown in Table 3, all nudge-states improve the load-carrying capacity and compliance of the PPPP panel, while the applied imperfection amplitude is less than the thickness of the shell. Most important, however, is the realisation that the original subcritical bifurcation has been converted into a supercritical one with a stable, imperfection-insensitive response. Hence, while the magnitude of the geometric modification made to the shell can be considered to be small, the method by which its shape is chosen leads to enhanced performance as compared to the general detrimental effect of stochastic imperfections or generic geometric alterations.

In the development of *well-behaved* nonlinear structures, large compliance is favoured, and modal nudging appears to significantly increase the compliance of shell structures. Owing to localised bending, the in-plane strain energy is transformed into out-of-plane bending energy, which results in an earlier onset of compliance (buckling-like) and significantly extends the subsequent region of stability. Furthermore, bending strains in thin-walled structures typically remain small, and hence yielding or plastic deformations are unlikely, even within the regime of increased compliance [27].

Note, that in all of the nudged responses there exists a small kink at around $\bar{R} = 0.5$, hence half the edge load of the first instability load of the baseline, unnudged panel. As a result, the panel transitions to a more compliant nonlinear regime earlier than the baseline design. Hence, modal nudging extends the stable post-buckling region of the shell by softening the originally stiff in-plane stiffness of the baseline shell. Reducing the nudging parameter value to bring the kink closer to $\bar{R} = 1$, *i.e.* the critical load at first instability for the un-nudged (baseline) panel, has the effect of breaking the pitchfork bifurcations, but the resulting equilibrium manifolds do not maintain stability throughout. Instead, there exist unstable regions immediately following the visible kink, which means the connection to the desired stable equilibria may occur via a dynamic snap.

4.2 Nudging a cylindrical panel: Clamped-Pinned (CCPP)

Six of the eight nudges applied to the CCPP panel use stable nudging states from the PPPP baseline response, and interestingly, all are shown to provide rewarding outcomes (Figures 11A–F and Table 3). In each case, the load-carrying capacity, compliance, and stable post-buckling response are improved with an applied imperfection smaller than the shell thickness. The greatest improvement for the CCPP panel is again observed for the nudge to state-VI, where, as illustrated in Figure 11F, a normalised load of $\bar{R} = 2.295$ and a compliance of $\bar{w} = 16.00$ is achieved. Interestingly, this nudge corresponds

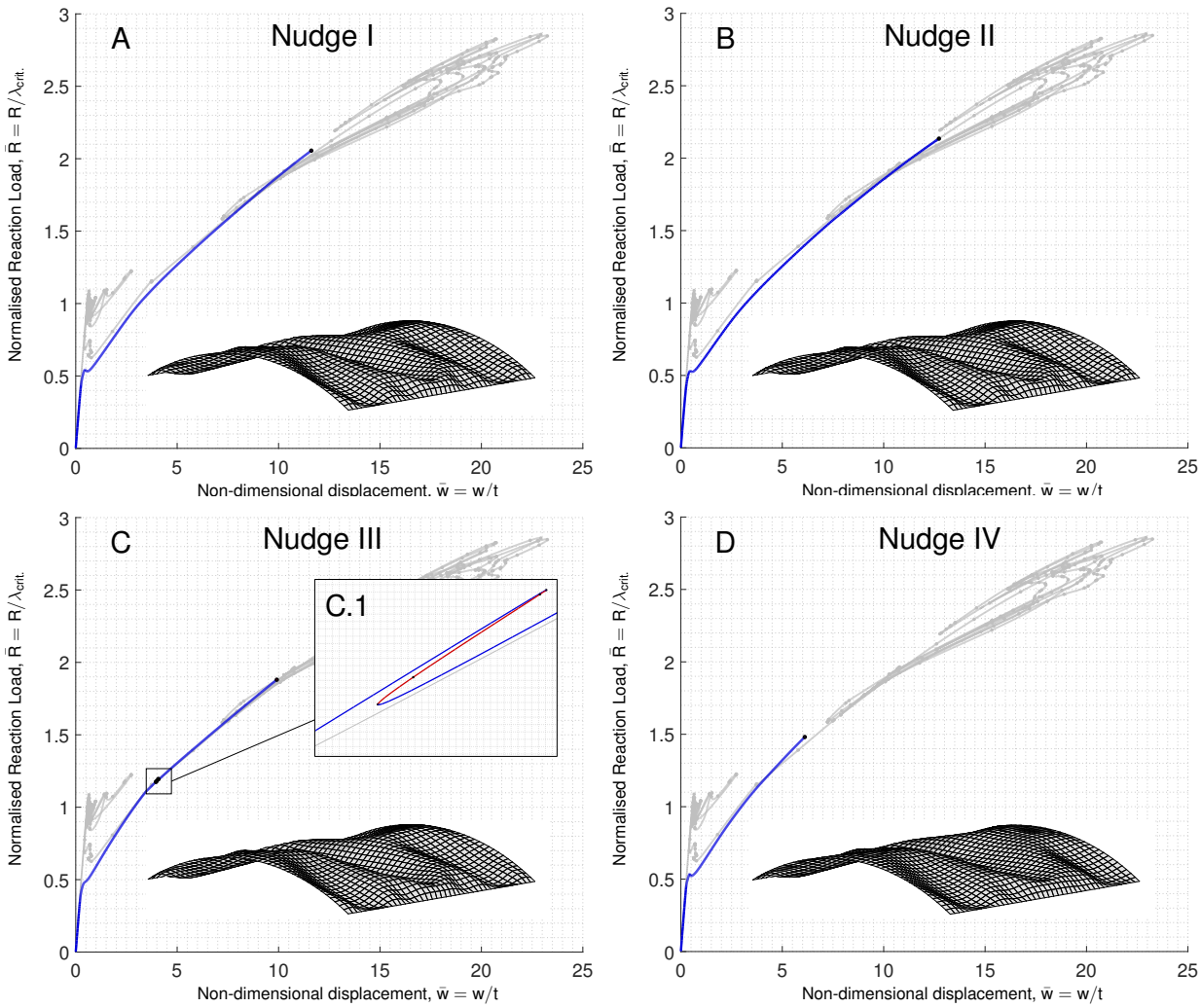

Fig. 10: Modal nudging the structural response of panel PPPP using states from the baseline response of PPPP. (A) Nudge-I, $\bar{u}_\eta = 0.760$ provides a successful nudge to a critical load of $\bar{R} = 2.056$; (B) Nudge-II, $\bar{u}_\eta = 0.844$ results in a successful nudge to a critical load of $\bar{R} = 2.135$; (C) Nudge-III, $\bar{u}_\eta = 0.941$ provides a successful nudge to an initial critical load of $\bar{R} = 1.194$, but also shows signs of potentially increasing to $\bar{R} = 1.880$; (D) Nudge-IV, with a nudging imperfection of $\bar{u}_\eta = 0.735$, a stable well-behaved response to a critical load of $\bar{R} = 1.481$ is achieved. The corresponding deformation mode shape is included for each response.

to the smallest geometry alteration of $\bar{u}_\eta = 0.488$, suggesting that this mode shape is the strongest attractor of all the modes evaluated.

As with all of the nudges carried out for both panels, there exists a kink in the response at the end of the initial linear phase. It is possible to completely remove this kink in order to recover a truly well-behaved response by increasing the nudge parameter. For values of η lower than presented in Table 3 a different response is observed. In this case, the nudge is sufficient to break many of the pitchfork bifurcations, but not sufficient to create a stable connection to the state of interest.

4.3 Modified geometry

The applied nudges described above modify the shell's behaviour as envisioned. However to further evaluate the robustness of these nudges we investigate the nudged response on perturbed geometries. Consider Figure 12, nudge state-II is applied to the PPPP shell, but with a $\pm 5\%$ variation in the original geometry of the shell. The variations considered are shell thickness, t, length, L, arc-length, s, and radius, r. It is evident in Figure 12 that the nudged response is robust and a successful response is observed for an identical nudging parameter value of $\eta = 16.5$. Figure 12A shows that a similar response is achieved for all of the alterations made to the initial geometry and Figure 12B provides a detailed illustration of these effects. It is clear that the change in thickness—equilibrium paths (1) and (9) in Figure 12—has the greatest effect on altering the structural response, and interestingly an increase in thickness has the opposite effect compared to an increase in

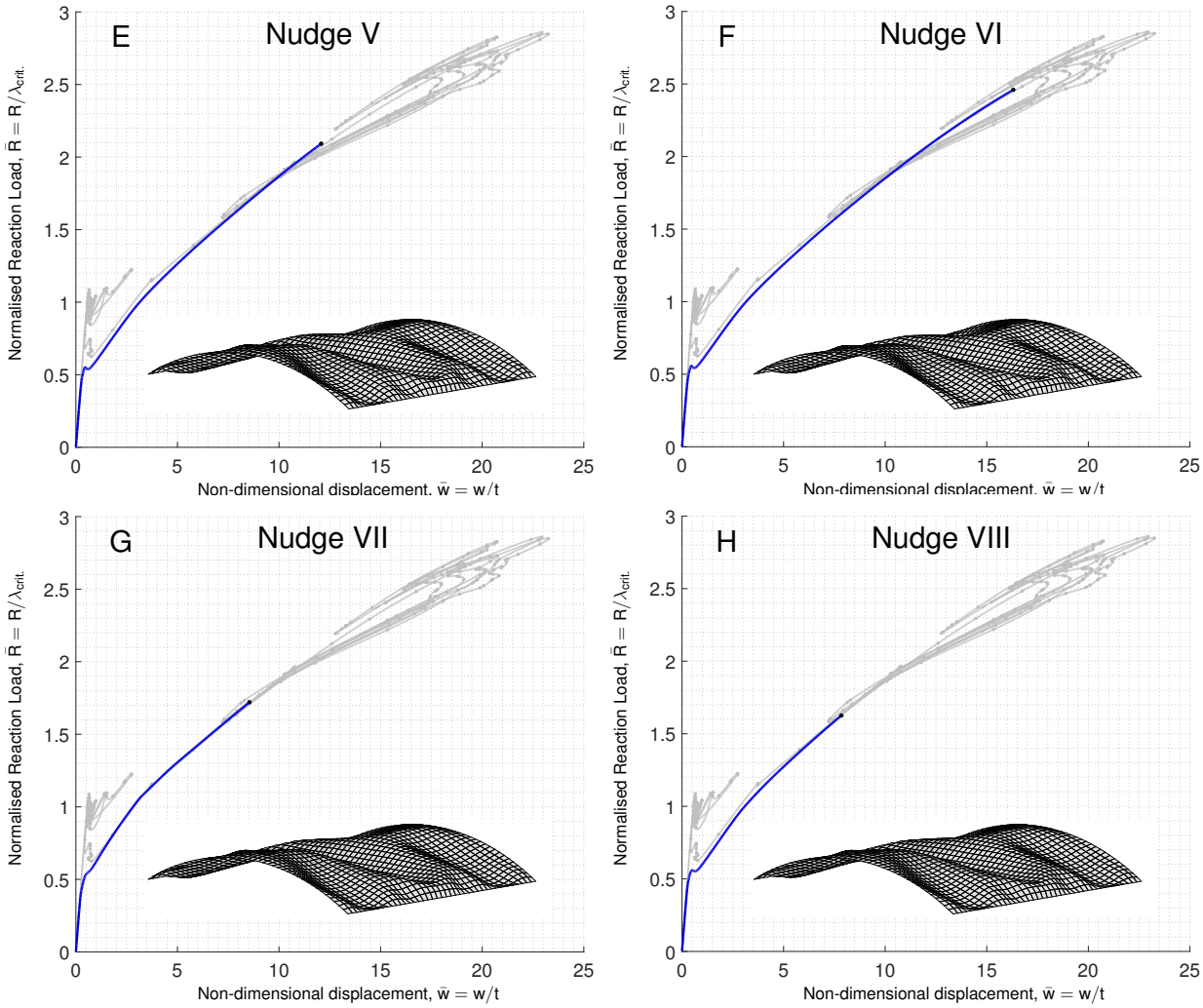

Fig. 10: Modal nudging the structural response of panel PPPP using states from the baseline response in PPPP and CCPP; (E) Nudge-V, $\bar{u}_\eta = 0.738$ provides a successful nudge to a critical load of $\bar{R} = 2.092$; (F) Nudge-VI, $\bar{u}_\eta = 0.745$ results in a successful nudge to a critical load of $\bar{R} = 2.460$; (G) Nudge-VII, with a nudging state from CCPP, and a value of $\bar{u}_\eta = 0.849$ provides a successful nudge to an initial critical load of $\bar{R} = 1.721$; (H) Nudge-VIII, with a nudging state from CCPP, and with a nudging imperfection of $\bar{u}_\eta = 0.702$, a stable well-behaved response to a critical load of $\bar{R} = 1.626$ is achieved. The corresponding deformation mode shape is included for each response.

any of the other parameters, *i.e.* the load carrying capacity increases with increased thickness, but the capacity reduces with increases in s, r, and L.

Figure 12C, however, highlights that there are two scenarios that do not recover the initially predicted nudged response. Equilibrium path (3) in Figure 12C is achieved by reducing the initial radius by 5%, and equilibrium path (6) is achieved by increasing the panel length L by 5%. For equilibrium path (3), the response clearly depicts a region of unstable equilibria within the largely stable response, and for equilibrium path (6) there is an unstable kink in the equilibrium path that, via a snapping phenomenon, could result in the exploitation of the full stable equilibrium path beyond. Furthermore, what is not shown in Figure 12C is the branching path emanating from the first branching bifurcation point on equilibrium path (3)—this path is stable and reconnects to the second branching point on the same path. Thus, even these relatively large changes in geometry (5%) have resulted in the creation of small portions of unstable equilibria, their effect on the structural behaviour is expected to be minimal as other stable states are readily encountered by small snaps or by branch switching. Overall, nudging is shown to be robust to geometric perturbations.

Although precisely controlling the proposed nudged seeded geometry in curvilinear geometry can pose quite a challenge, it has been shown in previous research on simpler beam structures [27], that only the dominant feature of the mode is sufficient to successfully "nudge" the structure. In this case, the imperfection magnitude increases to a multiple greater than the wall thickness, which certainly falls within the range of modern forming and 3D printing technologies. Furthermore,

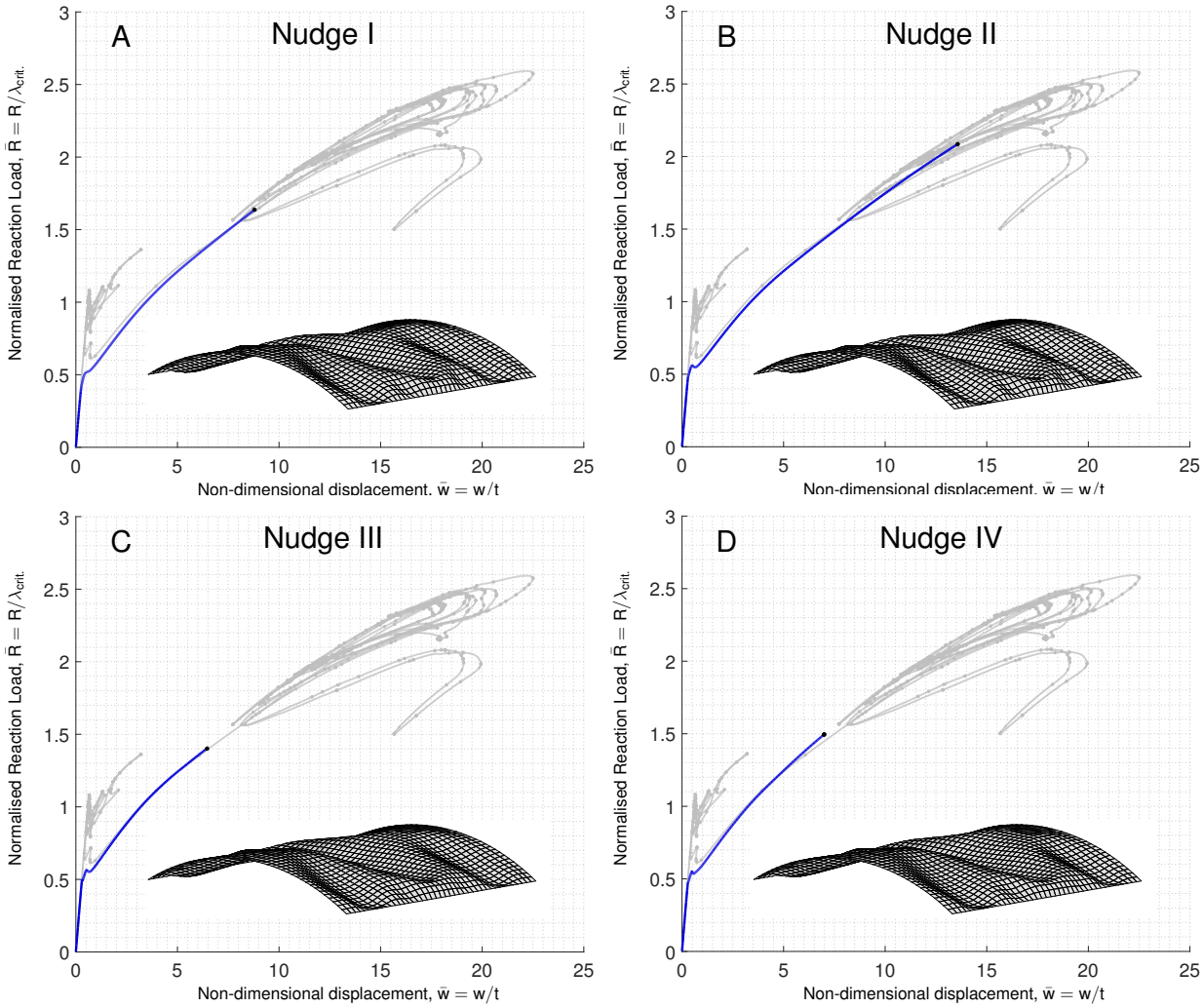

Fig. 11: Modal nudging the structural response of panel CCPP using states from the baseline response in PPPP. (A) Nudge-I, $\bar{u}_\eta = 0.760$ provides a successful nudge to a critical load of $\bar{R} = 1.637$; (B) Nudge-II, $\bar{u}_\eta = 0.563$ results in a successful nudge to a critical load of $\bar{R} = 2.085$; (C) Nudge-III, a value of $\bar{u}_\eta = 0.543$ provides a successful nudge to an initial critical load of $\bar{R} = 1.401$; (D) Nudge-IV, with a nudging imperfection of $\bar{u}_\eta = 0.601$, a stable well-behaved response to a critical load of $\bar{R} = 1.496$ is achieved. The corresponding deformation mode shape is included for each response.

owing to the fact that modal nudging marginally alters the stiffness of the structure via geometric modifications, the same effect should also be possible via the local modification of material properties, *i.e.* composite tow steering [36].

The magnitudes of the nudge modes defined herein are small in comparison to the characteristic thickness of the panels considered, and this undoubtedly provides limitations in terms of manufacturability. However, for the current panel the nudges impose an alteration to the initial geometry of 0.7–0.95 mm, therefore manufacturing does become feasible owing to the expected tolerances of modern 3D printing falling in the region of $\pm 50\,\mu$m and modern 3/5-axis CNC machining tolerances up to $\pm 25\,\mu$m.

Therefore, for the construction of small scale panels particularly relevant to experimentalists, 3D printing technologies could prove fruitful. At larger scales, 3/5-axis CNC machining process could be utilised to manufacture moulds for either a stamping/forming type process or alternatively for vacuum forming.

5 Spatial chaos in structures

Deterministic chaos traditionally refers to the irregular, unpredictable, and seemingly random behaviour of a deterministic dynamical system. Thompson and Virgin [37] and El Naschie and Al Athel [38] discuss the connection between the temporal chaos observed in the classic undamped oscillations of a pendulum and the "spatial" chaos of the planar elastica. The concept of spatial chaos in structures is defined by Kocsis and Károlyi [35] as the exponential increase in equilibrium

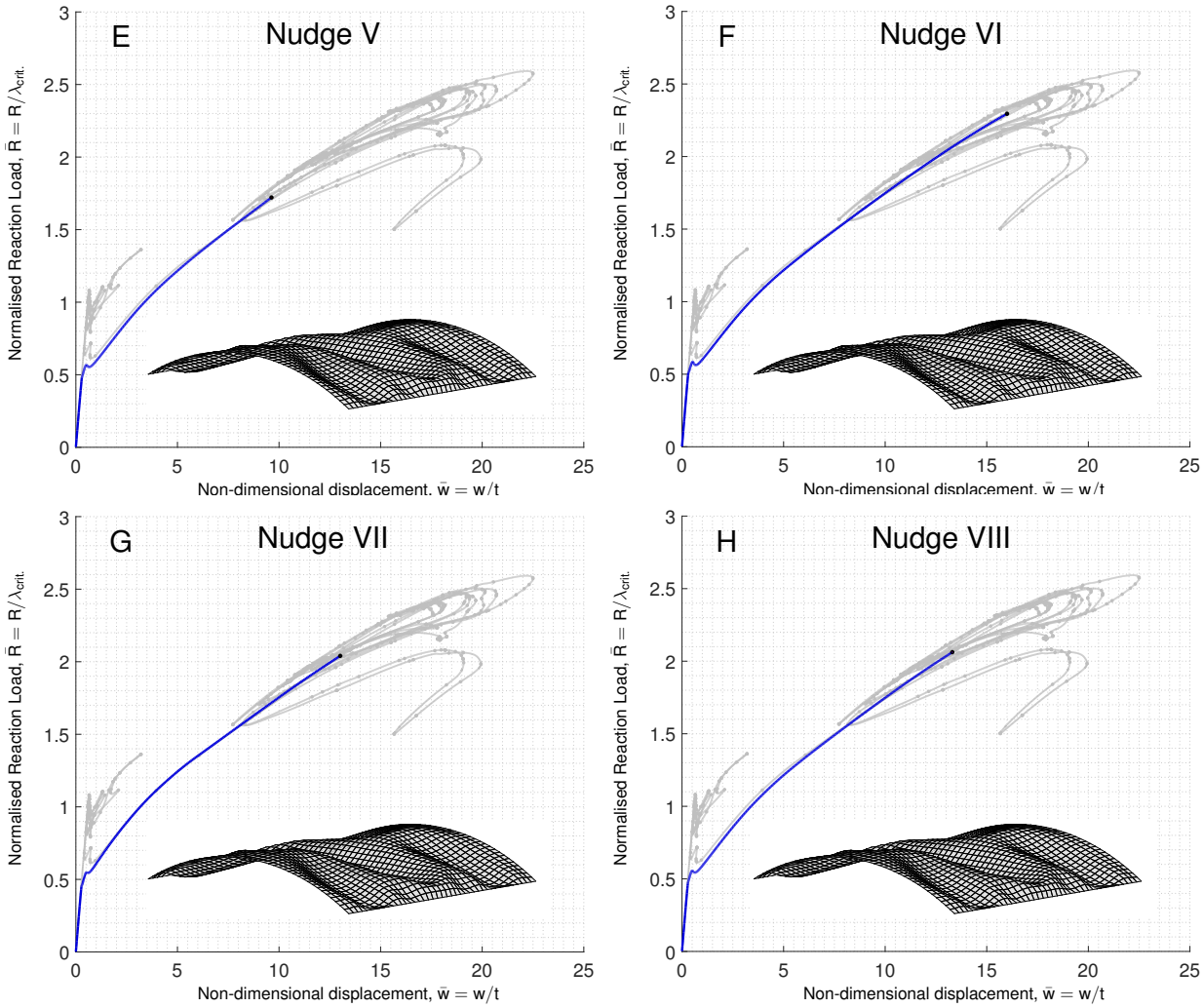

Fig. 11: Modal nudging the structural response of panel CCPP using states from the baseline response in PPPP and CCPP. (E) Nudge-V, $\bar{u}_\eta = 0.546$ provides a successful nudge to a critical load of $\bar{R} = 1.721$; (F) Nudge-VI, $\bar{u}_\eta = 0.488$ results in a successful nudge to a critical load of $\bar{R} = 2.295$; (G) Nudge-VII, with a nudging state from CCPP, and a value of $\bar{u}_\eta = 0.607$ provides a successful nudge to an initial critical load of $\bar{R} = 2.040$; (H) Nudge-VIII, with a nudging state from CCPP, and with a nudging imperfection of $\bar{u}_\eta = 0.562$, a stable well-behaved response to a critical load of $\bar{R} = 2.062$ is achieved. The corresponding deformation mode shape is included for each response.

paths as a result of continuous branching, which, as discussed by El Naschie and Al Athel [38], can result in localisations anywhere along the structure. This is particularly relevant to the present discussion and more specifically to the benefits of modal nudging.

To begin with, it is important to appreciate the connections made in Thompson and Virgin [37] and El Naschie and Al Athel [38] between spatial and temporal chaos. Consider an undamped rigid forced pendulum (see Figure 13A). Its motion is dynamic, as opposed to the quasi-static response of the elastica (see Figure 13B). The response of the forced pendulum and the imperfect elastica is mathematically described by the differential Eqs. 4a and 4b, respectively, and graphically by the stroboscopic map illustrated in Figure 13C.

$$mL\ddot{\theta} + mg\sin\theta = F\sin\omega t, \qquad \text{with} \qquad \ddot{\theta} = \frac{\partial^2\theta}{\partial t^2}, \tag{4a}$$

$$EI\ddot{\phi} + P\sin\phi = F\sin\omega s, \qquad \text{with} \qquad \ddot{\phi} = \frac{\partial^2\phi}{\partial s^2}. \tag{4b}$$

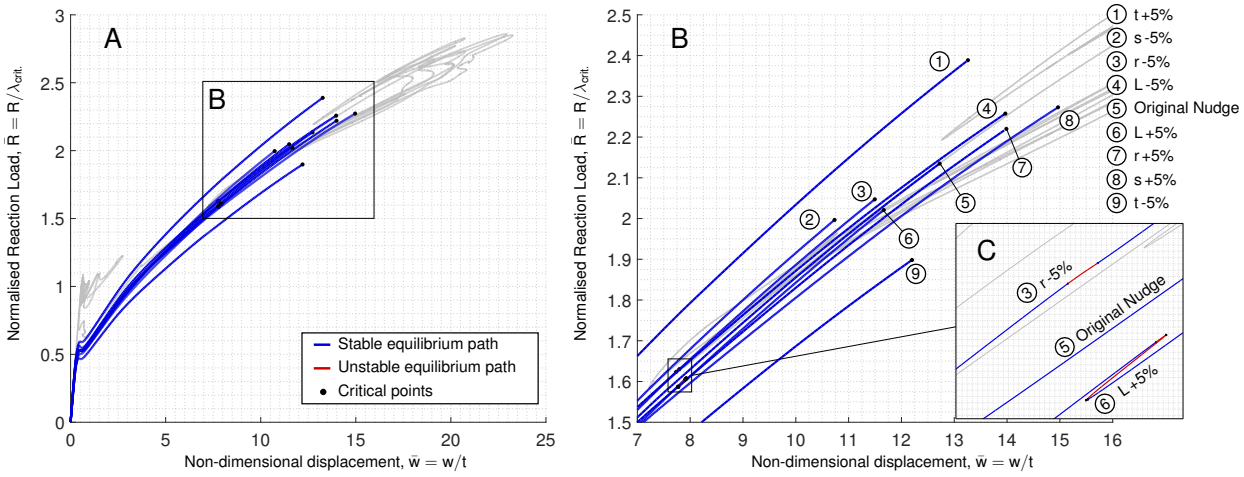

Fig. 12: Modal nudging the structural response of panel PPPP using state II with modifications made to the initial geometry of the panel. (A) The nudged response for each of the modifications made, a similar response is observed for all structural modifications, the nudging parameter $\eta = 16.5$ is identical for all responses. (B) A closer view of the variations observed in the structural response: (1) The panel thickness t is increased by 5%; (2) The panel arc-length s is reduced by 5%; (3) The panel radius is reduced by 5%; (4) The panel length L is reduced by 5%; (5) The original nudged response as illustrated in Figure 10B; (6) The panel length L is increased by 5%; (7) The panel radius r is increased by 5%; (8) The panel arc-length s is increased by 5%; (9) The panel thickness t is reduced by 5%. (C) Illustrates minor instabilities incurred for a reduction of the panel radius (3) and the increase in panel length (6). The other solutions have been removed from insert (C) for clarity.

Table 3: Results of nudging both PPPP and CCPP panels with eight different nudge states. The results shown are normalised critical load, normalised critical displacement, nudge parameter value and the corresponding maximum applied nudge-imperfection. η is the non-dimensional nudging parameter, $\bar{R} = R/\lambda_{\text{crit}}$ is the normalised total reaction load, $\bar{w} = w/t$ is the normalised end-shortening, and $\bar{u}_\eta = (\eta|\bar{\mathbf{u}}_{\text{state}}|)$ is the maximum geometric alteration.

	PPPP				CCPP			
Nudge	η	$\bar{R}$	$\bar{w}$	$\bar{u}_\eta$	η	$\bar{R}$	$\bar{w}$	$\bar{u}_\eta$
-	-	1	0.57	-	-	1	0.59	-
I	13.5	2.056	11.61	0.760	13.5	1.637	8.79	0.760
II	16.5	2.135	12.72	0.844	11	2.085	13.57	0.563
III	13	1.194	4.11	0.941	7.5	1.401	6.46	0.543
IV	11	1.481	6.11	0.735	9	1.496	7.00	0.601
V	13.5	2.092	12.07	0.738	10	1.721	9.63	0.546
VI	14.5	2.460	16.31	0.745	9.5	2.295	16.00	0.488
VII	10.5	1.721	8.54	0.849	7.5	2.040	13.01	0.607
VIII	12.5	1.626	7.84	0.702	10	2.062	13.31	0.562

Written in their current form, the two expressions presented in Eqs. 4a and 4b are analogous apart from Eq. 4a being a temporal initial-value problem and Eq. 4b a spatial boundary-value problem. In the former, m and L correspond to the end mass and pendulum length, respectively, θ is the angle of rotation and its second derivative $\ddot{\theta}$ is taken with respect to time t. In the latter, EI corresponds to the flexural rigidity of the elastica, P is the applied compressive force and ϕ is the curvature, with its second derivative $\ddot{\phi}$ taken with respect to the span s. In each equation, F is a measure of the perturbation amplitude and ω is the measure of the spatial or temporal frequency. As the temporal variable t ranges from zero to infinity, a formal analogy between the initial-value problem of the pendulum and the boundary-value problem of the elastica requires the assumption that $s \to \infty$.

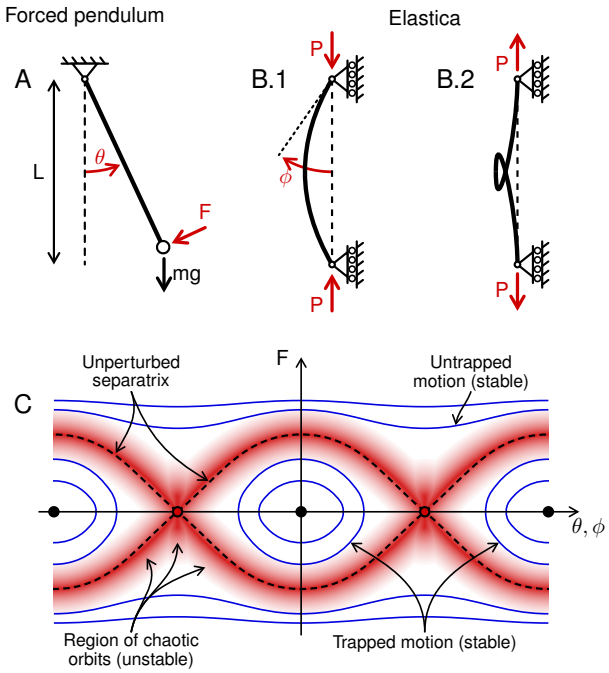

Fig. 13: (A) Forced pendulum; (B.1) Buckled elastica; (B.2) Single loop of buckled elastica; (C) Conceptual stroboscopic map (Poincaré phase portrait). The forced pendulum is capable of exhibiting controlled and predictable behaviour provided that the applied force F is small. In this scenario, the motion is such that the pendulum swings back and forth in a predictable manner, corresponding to the trapped motion in (C). However, when the applied perturbation F is large, the motion of the pendulum is such that it revolves continuously about its pinned end, corresponding to the untrapped stable regions in (C). At some point between these two scenarios the motion of the pendulum becomes temporally chaotic, corresponding to the red regions of chaotic orbits in (C). Analogously, assuming an infinitely long elastica—where the arc-length variable s replaces the temporal variable t—shows signs of spatial chaos for small imperfection amplitudes. In (B.2) we see only one loop, however for an infinitely long elastica many loops would generate at arbitrary and unpredictable locations. For large imperfections, it is possible to accurately predict the deformation of the structure corresponding to the untrapped stable solution in (C).

For $F = 0$, the motion of the pendulum is controlled and corresponds to the trapped motion illustrated in Figure 13C. This homoclinic orbit represents the pendulum swinging from a perfectly inverted position down and back to its starting point. Similarly for the elastica, the case $F = 0$ corresponds to a perfect (imperfection free) elastica, and the homoclinic solution analogous to the fully inverted pendulum is a single loop generated at the midspan as illustrated in Figure 13B.2. This deformation can be thought of as a grossly post-buckled example of the elastica presented in Figure 13B.1, whereby the loaded ends have passed through one another.

For large values of F, the motion of the pendulum is also controlled and corresponds to the untrapped motion illustrated in Figure 13C. This physically represents the pendulum swinging continuously in one direction around the central pin. Similarly for the elastica, large F corresponds to large spatial imperfections with fundamentally altered geometry. This corresponds to the elastica being forced into a specific looping sequence corresponding to the strong influence of the initial imperfection.

In both cases (temporal and spatial), an intermedial value of F may result in a chaotic response, which is highlighted in red in Figure 13C. For the forced pendulum, within a critical range of values, the influence of the forcing term F causes a deterministic sequence of oscillations that is highly sensitive to the starting conditions (θ and $\dot{\theta}$ in the initial-value problem). In the case of the elastica, localised post-buckling solutions (loops) may form at one or multiple locations along the length, and the exact sequence/position of these is strongly dependent on the initial sinusoidal imperfection.

Although the cylindrical panels considered here are of finite length, the static-dynamic analogy nevertheless provides some physical insight into the relation of stochastic imperfections and modal nudging. Due to the large number of unstable post-buckling paths, there exist many escape routes from the pre-buckling path that act as attractors depending on the form of the initial imperfections. As the precise shape of stochastic imperfections is generally unknown, it is hard to quantify which unstable post-buckling path will be the dominant attractor. By using modal nudging, a specific attractor is chosen *a priori* such that these seeded geometries drive the structure into a particular post-buckling response.

6 Conclusion

The response of two axially-compressed cylindrical shell panels was studied by means of a displacement-controlled finite element procedure. One panel was pinned on all four edges (PPPP) and the other was clamped at the two curved ends to prevent rotation on the loaded edges (CCPP). By making use of numerical continuation procedures, we present new insights into the complexity of the characteristics of stability of the shell by providing a comprehensive exploration of the post-buckled structural response. The observed complexity shows signs of "spatial" chaos with a vast number of critical points, entangled equilibrium paths and an exponentially increasing number branching points.

Furthermore, we uncover a number of stable equilibrium solution paths deep in the post-buckling regime that are more desirable—in terms of increased load-carrying capacity, increased compliance or increased stability—than the baseline response of the PPPP and CCPP panels. It is possible to exploit the inherent advantages of these desirable stable solution paths by employing the previously introduced modal nudging technique, which modifies the baseline geometry based on the mode shapes of the desirable stable solutions.

By using modal nudging, well-behaved shell structures are recovered whose load-carrying capacity, compliance and stability are improved when compared directly to the original structure. It is noted that the post-buckled response from one structure (*e.g.* PPPP) can also be used to improve the response of the other (*e.g.* CCPP). For both PPPP and CCPP, the greatest increase in compliance and load-carrying capacity was observed for nudge-VI, which corresponds to a state from the post-buckled regime of PPPP.

Modal nudging involves a minor alteration of the original undeformed shell geometry. The panel's load-carrying capacity can be increased by 246% and 229.5% for PPPP and CCPP, respectively, when compared to their original response. Furthermore, increases in normalised compliance from 0.57 to 16.31 and from 0.59 to 16.00 is respectively observed for the PPPP and CCPP panels. These gains of load-carrying capacity and compliance are generated from an alteration to the original geometry exceeding no more than 75% of the total thickness for the PPPP panel, and 49% of the total thickness for the CCPP panel, which equates to a geometry change of only 0.75 mm and 0.49 mm, respectively. Most importantly, all nudges to desirable states transformed the bifurcation behaviour of the shells from subcritical to supercritical, thereby eliminating imperfection sensitivity. However, this improved performance in terms of load-carrying capacity, compliance and stability comes at the cost of an earlier onset of nonlinearity compared to the baseline designs.

Additional design drivers, such as the yield limit, were not taken into account during this work owing to the fact that the additional compliance is derived from localised bending as opposed to in-plane strain energy. However, these are factors to consider to uncover more practical stable shell designs. This will be a topic for future research.

Acknowledgements

BSC is supported by the Engineering and Physical Sciences Research Council (EPSRC) through the EPSRC Centre for Doctoral Training in Advanced Composites in Innovation and Science [grant number EP/G036772/1]. AP is supported by the EPSRC Fellowship scheme [grant number EP/M013170/1]. RMJG is supported by the Royal Academy of Engineering under the Research Fellowship scheme [grant number RF\201718\17178]. The support of all funders is gratefully acknowledged.

Data statement

All data required to reproduce the figures in this paper can be found on the data repository of the University of Bristol via URL: https://doi.org/10.5523/bris.1fdbdk006dcth2n9ky8vlfwj7l.

References

[1] P.M. Reis. A perspective on the revival of structural (in)stability with novel opportunities for function: From buckliphobia to buckliphilia. *Journal of Applied Mechanics*, 82(11):111001–1–11001–4, 2015.

[2] N. Hu and R. Burgueño. Buckling-induced smart applications: recent advances and trends. *Smart Materials and Structures*, 24:1, 2015.

[3] R.M.J. Groh, D. Avitabile, and A. Pirrera. Generalised path-following for well-behaved nonlinear structures. *Computer Methods in Applied Mechanics and Engineering*, 331:394–426, 2018.

[4] A. Pirrera, D. Avitabile, and P.M. Weaver. Bistable plates for morphing structures: A refined analytical approach with high-order polynomials. *International Journal of Solids and Structures*, 47:3412–3425, 2010.

[5] G. Arena, R.M.J. Groh, A. Brinkmeyer, R. Theunissen, P.M. Weaver, and A. Pirrera. Adaptive compliant structures for flow regulation. *Proceedings of the Royal Society of London A: Mathematical, Physical and Engineering Sciences*, 473(2204):20170334, August 2017.

[6] B. Andò, S. Baglio, C. Trigona, N. Dumas, L. Latorre, and P. Nouet. Nonlinear mechanism in mems devices for energy harvesting applications. *Journal of Micromechanics and Microengineering*, 20(12):125020, 2010.

[7] S.P. Pellegrini, N. Tolou, M. Schenk, and J.L. Herder. Bistable vibration energy harvesters: A review. *Journal of Intelligent Material Systems and Structures*, 24(11):1303–1312, May 2012.

[8] S.A. Alkharabsheh and M.I. Younis. Statics and dynamics of mems arches under axial forces. *Journal of Vibrations and Acoustics*, 135(021007):1–7, 2013.

[9] J. Arbocz and J.H. Starnes Jr. Future directions and challenges in shell stability analysis. *Thin-Walled Structures*, 40: 729–754, 2002.

[10] W.T. Koiter. *The Stability of Elastic Equilibrium*. PhD thesis, Techische Hooge School at Delft, 1945.

[11] J. Arbocz and C.D. Babcock. The effects of general imperfections on the buckling of cylindrical shells. *Journal of Applied Mechanics*, 36(1):28–38, 1969.

[12] Y.C. Song, J.G. Teng, and J.M. Rotter. Imperfection sensitivity of thin elastic cylindrical shells subject to partial axial compression. *International Journal of Solids and Structures*, 41:7155–7180, 2004.

[13] F.L. Jiménez, J. Marthelot, A. Lee, J.W. Hutchinson, and P.M. Reis. Technical brief: Knockdown factor for the buckling of spherical shells containing large-amplitude geometric defects. *Journal of Applied Mechanics*, 84(3):034501–1 – 034501–4, 2017.

[14] H.A. Mang, C. Schranz, and P. Mackenzie-Helnwein. Conversion from imperfection-sensitive into imperfection-insensitive elastic structures. i: Theory. *Computer Methods in Applied Mechanics and Engineering*, 195:1422–1457, 2006.

[15] C. Schranz, B. Krenn, and H.A. Mang. Conversion from imperfection-sensitive into imperfection-insensitive elastic structures. ii: Numerical investigation. *Computer Methods in Applied Mechanics and Engineering*, 195:1458–1479, 2006.

[16] X. Ning and S. Pellegrino. Imperfection-insensitive axially loaded thin cylindrical shells. *International Journal of Solids and Structures*, 62:39–51, 2015. ISSN 0020-7683.

[17] X. Ning and S. Pellegrino. Experiments on imperfection insensitive axially loaded cylindrical shells. *International Journal of Solids and Structures*, 115-116:73–86, 2017.

[18] R. Burgueño, N. Hu, A. Heeringa, and N. Lajnef. Tailoring the elastic postbuckling response of thin-walled cylindrical composite shells under axial compression. *Thin-Walled Structures*, 84:14–25, 2014.

[19] N. Hu, R. Burgueño, and N. Lajnef. Structural optimization and form-finding of cylindrical shells for targeted elastic postbuckling response. In *Proceedings of the ASME 2014 Conference on Smart Materials, Adaptive Structures and Intelligent Systems*, 2014.

[20] N. Hu and R. Burgueño. Tailoring the elastic postbuckling response of cylindrical shells: A route for exploiting instabilities in materials and mechanical systems. *Extreme Mechanics Letters*, 4:103–110, 2015.

[21] N. Hu and R. Burgueño. Elastic postbuckling response of axially-loaded cylindrical shells with seeded geometric imperfection design. *Thin-Walled Structures*, 96:256–268, 2015.

[22] N. Hu and R. Burgueño. Harnessing seeded geometric imperfection to design cylindrical shells with tunable elastic postbuckling behavior. *Journal of Applied Mechanics*, 84:011003, 2017.

[23] S.C. White and P.M. Weaver. Towards imperfection insensitive buckling response of shell structures: Shells with plate-like post-buckled responses. *The Aeronautical Journal*, 120(1224), 2016.

[24] J. Bielski. A global plasticity formulation combined with a semi-analytical analysis of imperfect shells of revolution. *Thin-Walled Structures*, 23(1):399–411, 1995. ISSN 0263-8231. Buckling Strength of Imperfection-sensitive Shells.

[25] Z. Lu, H. Obrecht, and W. Wunderlich. Imperfection sensitivity of elastic and elastic-plastic torispherical pressure vessel heads. *Thin-Walled Structures*, 23(1):21–39, 1995. ISSN 0263-8231. Buckling Strength of Imperfection-sensitive Shells.

[26] A. Lee, F.L. Jiménez, J. Marthelot, J.W. Hutchinson, and P.M. Reis. The geometric role of precisely engineered imperfections on the critical buckling load of spherical elastic shells. *Journal of Applied Mechanics*, 83(11):111005–1

– 11005–11, 2016.
[27] B.S. Cox, R.M.J. Groh, D. Avitabile, and A. Pirrera. Modal nudging in nonlinear elasticity: Tailoring the elastic post-buckling behaviour of engineering structures. *Journal of the Mechanics and Physics of Solids*, 116:135–149, July 2018.
[28] S.M. Jun and C.S. Hong. Buckling behaviour of laminated composite cylindrical panels under axial compression. *Computers and Structures*, 29(3):479–490, 1988.
[29] E. Ramm. A plate/shell element for large deflections and rotations. In K. J. Bathe, T. Oden, and W. Wunderlich, editors, *Formulations and Computational Algorithms in Finite Element Analysis*, Formulations and Computational Algorithms in Finite Element Analysis. MIT Press, Boston MA, 1977.
[30] E. Riks. The application of newton's method to the problem of elastic stability. *Journal of Applied Mechanics*, 39(4): 1060–1065, 1971.
[31] R.M. Neville, R.M.J. Groh, A. Pirrera, and M. Schenk. Shape control for experimental continuation. *Physical Review Letters*, 120:254101, 2018.
[32] R.M.J. Groh and A. Pirrera. Orthotropy as a driver for complex stability phenomena in cylindrical shell structures. *Composite Structures*, 198:63–72, 2018.
[33] R.M.J. Groh and A. Pirrera. Extreme mechanics in laminated shells: New insights. *Extreme Mechanics Letters*, 23: 17–23, 2018.
[34] J.M.T. Thompson. Advances in shell buckling: Theory and experiments. *International Journal of Bifurcation and Chaos*, 25(1):1–25, 2015.
[35] A. Kocsis and G. Károlyi. Conservative spatial chaos of buckled elastic linkages. *Chaos: An Interdisciplinary Journal of Nonlinear Science*, 16(3):033111, 2006.
[36] Z. Gürdal, B.F. Tatting, and C.K. Wu. Variable stiffness composite panels: Effects of stiffness variation on the in-plane and buckling response. *Composites Part A Applied Science and Manufacturing*, 39:911–922, 2008.
[37] J.M.T. Thompson and L.N. Virgin. Spatial chaos and localization phenomena in nonlinear elasticity. *Physics Letters A*, 126(8-9):491–496, January 1988.
[38] M.S. El Naschie and S. Al Athel. On the connection between statical and dynamical chaos. *Zeitschrift für Naturforschung A*, 44(7), January 1989.